Monthly Notices of the ROYAL ASTRONOMICAL SOCIETY

MNRAS **498,** 2688–2696 (2020) doi:10.1093/mnras/staa2383
Advance Access publication 2020 August 31

HP Cet and Swift J0820.6–2805: two candidate intermediate polars observed by *XMM–Newton*

A. A. Nucita,[1,2]★ F. De Paolis,[1,2] F. Strafella[1,2] and D. Licchelli[3,4]

[1]*Department of Mathematics and Physics 'E. De Giorgi', University of Salento, Via per Arnesano, CP-I93, I-73100 Lecce, Italy*
[2]*INFN, Sezione di Lecce, Via per Arnesano, CP-193, I-73100 Lecce, Italy*
[3]*R.P. Feynman Observatory, Gagliano del Capo, I-73034 Lecce, Italy*
[4]*CBA, Center for Backyard Astrophysics, Gagliano del Capo, I-73034 Lecce, Italy*

Accepted 2020 August 6. Received 2020 July 28; in original form 2020 June 22

ABSTRACT

We report on the *XMM–Newton* observation of HP Cet and Swift J0820.6–2805, two X-ray photon sources that are candidates to be members of the intermediate polar class of cataclysmic variables. If the historical optical light curve of HP Cet shows a periodic feature at $\simeq$96 min, a clear identification of such a signature in the high energy band (apart for a variability on a time-scale of $\simeq$8 min as detected by the *ROSAT* satellite) is lacking. By using *XMM–Newton* archive data, we clearly identify a feature (at $\simeq$88 min) which is marginally consistent with one of the binary system orbital periods reported in the literature. We also found a signature of a periodic features on the time-scale of $\simeq$5.6 min. In the case of Swift J0820.6–2805, the intermediate polar nature was previously unclear and the orbital and the white dwarf spin periods were unknown. Here, the 0.3–10 keV data undoubtedly reveal an orbital period and a white dwarf spin of $\simeq$87.5 and $\simeq$27.9 min, respectively. The spectral analysis showed that both HP Cet and Swift J0820.6–280 are members of the underluminous IP subclass since their luminosity in the 0.3–10 keV band is estimated to be $\simeq 5 \times 10^{30}$ and $\simeq 3.8 \times 10^{29}$ erg s^{-1}, respectively.

Key words: novae, cataclysmic variables – white dwarfs – X-rays: binaries – X-rays: individual: HP Cet – X-rays: individual: Swift J0820.6–2805.

1 INTRODUCTION

A binary system made of a white dwarf (WD) primary accreting material from a donor star constitutes what is commonly known as a cataclysmic variable (hereinafter CV; see e.g. Kuulkers et al. 2006 for a review).

CVs come in three different flavours, depending on the details of the accretion mechanism and the strength of the magnetic field. In particular, non-magnetic systems (with a field $\lesssim$0.1 MG, see e.g. van Teeseling, Beuermann & Verbunt 1996; Nucita et al. 2009a,b, 2011, 2014; Hoard et al. 2010; Balman 2011; Mukai 2017) constitute the *dwarf novae* class. Conversely, large magnetic field objects (with magnetic field strength exceeding 10 MG, see e.g. Ramsay et al. 2004; Szkody et al. 2004) are known as *polars*. CVs characterized by a magnetic field value between the previous two extrema specify the subset of *intermediate polars* or IPs.

In IPs (see e.g. Worpel et al. 2020 for a recent analysis of a sample of newly confirmed IPs), the accreted material suffers of a shock wave close to the WD surface and, as a consequence, it releases hard X-ray photons that, once detected, can be used to study in detail the accretion process. IP candidates are found by using optical and/or X-ray observations by means of the identification of emission lines and the characteristics of the high energy spectrum.

Often the high energy signal is modulated (Parker et al. 2005) on the WD spin $P_{\rm spin}$, the orbital period $P_{\rm orb}$ as well as on the synodic period $P_{\rm syn}$ (i.e. $P_{\rm syn}^{-1} = P_{\rm spin}^{-1} - P_{\rm orb}^{-1}$) due to the presence of reprocessing sites. Hence, the existence of multiple periodic components is a signature that IPs are intrinsically different from the more strongly magnetic polars in which the WD spin and the orbital period are synchronized.

In fact, as pointed out by Warner (1995), when one considers that the X-ray production site is characterized by a variable geometry as seen by the observer, multiple orbital sidebands are found and naturally expected. Hence, the power spectrum is expected to host features at the additional peculiar frequencies $P_{\rm spin}^{-1} \pm P_{\rm orb}^{-1}$ and $P_{\rm spin}^{-1} \pm 2P_{\rm orb}^{-1}$ due to amplitude modulation at $P_{\rm orb}$ and $2P_{\rm orb}$.

As noted by Nucita, Conversi & Licchelli (2019; but see also Worpel et al. 2020), in the case of the IP DW Cnc, detecting (in the Fourier power spectrum of X-ray data) signatures of the orbital and spin periods, together with the associated multiple sidebands is a powerful method for classifying a CV as a member of the IP class. Therefore, dedicated X-ray campaigns with sufficient sensitivity are crucial for a correct classification of such objects.

IPs are expected to be quite common in the Galaxy and are thought to significantly contribute to the overall X-ray ridge background. In fact, it is known that much of the Galactic ridge X-ray background (a diffuse emission which is observed to be concentrated around the Galactic plane, see Worrall et al. 1982), is still without an exhaustive explanation. The issue was partly solved by using Chandra X-ray observations (Revnivtsev et al. 2009), which showed that

★ E-mail: nucita@le.infn.it

$\simeq$80 per cent of the signal is resolved in many faint point sources, including IPs which dominate (Warwick, Byckling & Pérez-Ramírez 2014) for energy above $\simeq$10 keV. However, only about *sixty* sources have been classified as IPs so far (see e.g. the most updated IP catalogue -*IPhome*- available at https://asd.gsfc.nasa.gov/Koji.Mukai/iphome/iphome.html). Therefore, dedicated survey and follow-up observations, with the aim to discover and study this population of objects, would be required.

Here, we report on the timing analysis of X-ray data from two CVs, HP Cet and Swift J0820.6–2805. These sources are IP candidates and are present in the IPhome list where their IP nature is reported as *doubtful* and *possible*, respectively. Furthermore, the *XMM–Newton* observations for HP Cet (ID 673140201) and Swift J0820.6–2805 (ID 0801780401) were not previously analyzed. In particular, for Swift J0820.6–2805, a confirmation of the IP nature and the identification of the orbital and spin periods are still lacking.

For HP Cet, our analysis of the 0.3–10 keV band data, as well as the UV light curve, confirms the existence of what we tentatively identify as the orbital modulation at $\simeq$88 min (slightly different from the value of $\simeq$96 min reported by Southworth et al. 2006). We further detect a periodic feature at $\simeq$5.6 min that is close to variability of about 8 min (Szkody et al. 2002), estimated on the basis of *ROSAT* satellite data.

In the case of the IP candidate Swift J0820.6–2805, we showed that the high energy light curve is characterized by a modulation on what we identify to be the orbital period of $\simeq$87.5 min. Searching for the typical sidebands expected for IPs resulted in the clear identification of the spin period at $\simeq$27.9 min. Thus, the period search allowed us to confirm the IP nature of the source.

2 THE *XMM–NEWTON* VIEW OF HP CET AND SWIFT J0820.6–2805

2.1 Data reduction

HP Cet (with J2000 coordinates RA = $02^{h}33^{m}22\overset{s}{.}61$ and Dec. = $+00^{\circ}50'59\overset{''}{.}5$) was observed by the *XMM–Newton* satellite in 2012 (Observation ID 0673140201) for $\simeq$22.5 ks. The observation started (ended) on 2012 January 15 at 21: 24: 20 (03: 39: 33) UT. The source was pointed by the EPIC pn and MOS cameras operating in full frame mode and with medium filter as well as by the Optical Monitor (OM) in image and fast mode. The adopted filter is the *UVM2*, which offers a bandpass centred at $\simeq$231 nm.

Swift J0820.6–2805 (also known as 1RXS J082033.6–280457 and PBC J0820.4–2801 with J2000 coordinates RA = $08^{h}20^{m}34\overset{s}{.}11$ and Dec. = $-28^{\circ}04'58\overset{''}{.}8$) was discovered by means of the Swift survey (Baumgartner et al. 2013). A bright counterpart was identified in the UV (Cusumano et al. 2010) and recognized as a possible IP by Parisi et al. (2014) via the identification of prominent lines of H, He I, and He II. The source was observed by the *XMM–Newton* satellite as a part of a larger follow-up program. The target was observed in 2018 (ID 801780401) by the EPIC cameras operating in small window mode and thin filter. The OM observed the target in image and fast mode with the adoption of the *B* filter centred at 450 nm. The observation lasted for $\simeq$37 ks.

The EPIC raw data files (ODFs) were processed using the XMM-SAS (Science Analysis System version 17.0.0) using the latest calibration constituent files (CCFs). We obtained the calibrated event list files for the three EPIC cameras by running the SAS tasks *emchain* and *epchain*. We corrected the event files for the Solar system barycenter (via the *barycen* SAS tool) in order to convert the photon arrival times from spacecraft time to the barycentric dynamical time.

We then searched for segments of each observation affected by soft proton flares in order to determine a list of good time intervals (GTIs) to be applied in the following spectral and timing analysis. Note, however, that while the observation of Swift J0820.6–2805 were not disturbed by flares,[1] HP Cet was affected by strong flares for $\simeq$ 45 per cent of the observation duration. In the latter case, we decided to be as restrictive as possible and concentrate only on the first $\simeq$9 ks which were not affected by flares.[2] Obviously, this strongly reduces our capability to test periods larger than $\simeq$50 min.[3]

GTIs were also considered for the spectral analysis of the source. We also generated 0.3–10 keV images for inspecting purposes (see e.g. Figs 1a and b, where we give a zoom around the nominal target coordinates). In each case, the source (plus background) count rate was extracted in the soft (0.3–2 keV), hard (2–10 keV), and full (0.3–10 keV) bands by adopting a circular region with radius of 40 arcsec, which guarantees the possibility to collect $\simeq$88 per cent of the total energy. The source extraction region was positioned on the nominal target coordinates while the background photons are extracted in circular regions (with radius of $\simeq$80 arcsec) placed on the same chip but far from any other visible source.

For each band and for each instrument, we first extracted the source time-series, we searched for the maximum overlapping time interval and then flagged the common start and stop times. We then produced synchronized light curves with bin size of 10, 60, and 120 s and repeated the whole procedure for the background. Finally, we used the *epiclccorr* task to get the final MOS 1, MOS 2, and pn source (background subtracted and synchronized) time series that were then averaged bin-by-bin. The light curves were then scaled in time in order to start from 0. In Figs 2a and b, we give the soft, hard, and full X-ray light curves for the sources of interest, with the medium and hard light curves appearing more noisy.

The OM *UVM2* (for HP Cet) and *B* (for Swift J0820.6–2805) data were extracted by using the standard SAS task OMFCHAIN. The bin size of each light curve[4] was set to 10 s.

Finally, we extracted the spectrum for the source and the background by using the same regions described above and requiring to have at least 25 counts per energy bin. The source and background spectra as well as the associated response matrices and ancillary files were then used within the XSPEC software (version 12.9.0) to account for the spectral analysis and the estimate of the 0.3–10 keV band flux.

2.2 Timing analysis in the X-rays

For each source target of this study, the barycentric and background corrected light curves were extracted (and synchronized) in the soft (0.3–2 keV) and hard (2–10 keV) bands with several bin of 10, 60, and 120 s (see Fig. 2).

[1] The net count rate remains in all the cameras always below 0.4 count s^{-1} for photons with energy larger than 10 keV.

[2] In order to exploit the full observation, we attempted a procedure avoiding the application of GTIs. Indeed, since any background extraction region is affected by soft proton flares similarly to what happens for the source, after a proper subtraction (bin by bin) of the synchronized light curves one is left with the full source light curves. We note that this approach introduces too many spurious features that are *unstable* versus a time resolved periodogram. Thus, this possibility is not explored further in the rest of this paper.

[3] The upper limit on the period that can be tested derives from our request to have at least three full cycles in the time series.

[4] The zero-point magnitudes for the OM *UVM2* and *B* filter are 15.7724 and 19.2661, respectively (XMM User Guide 2019).

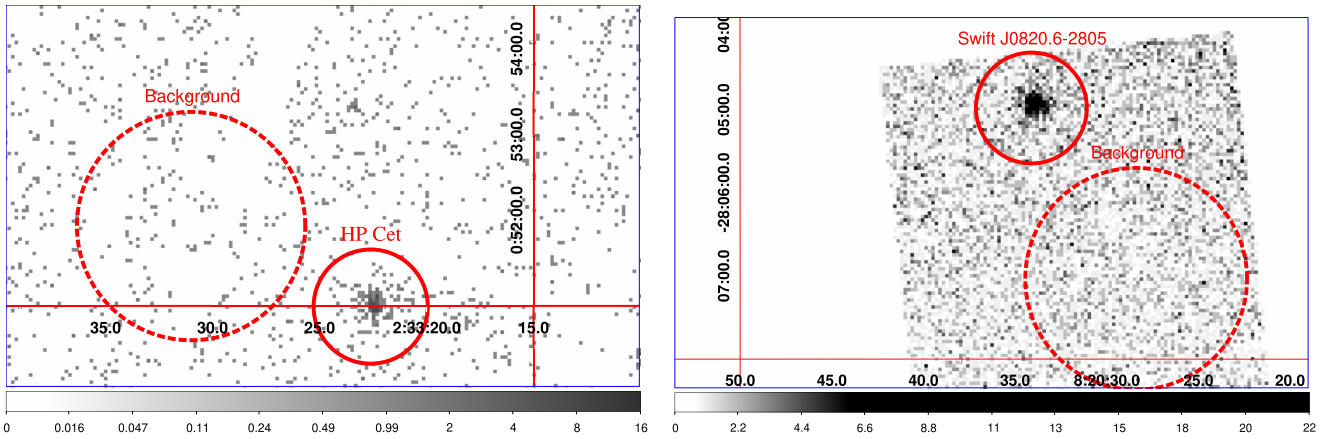

(a) (b)

Figure 1. Images in the 0.3–10 keV band were extracted as described in the text. In yje figure, we give a zoom around the nominal coordinates of the target: HP Cet is on the left-hand panel (MOS 1 camera), while Swift J0820.6–2805 is shown on the pn camera (right-hand panel).

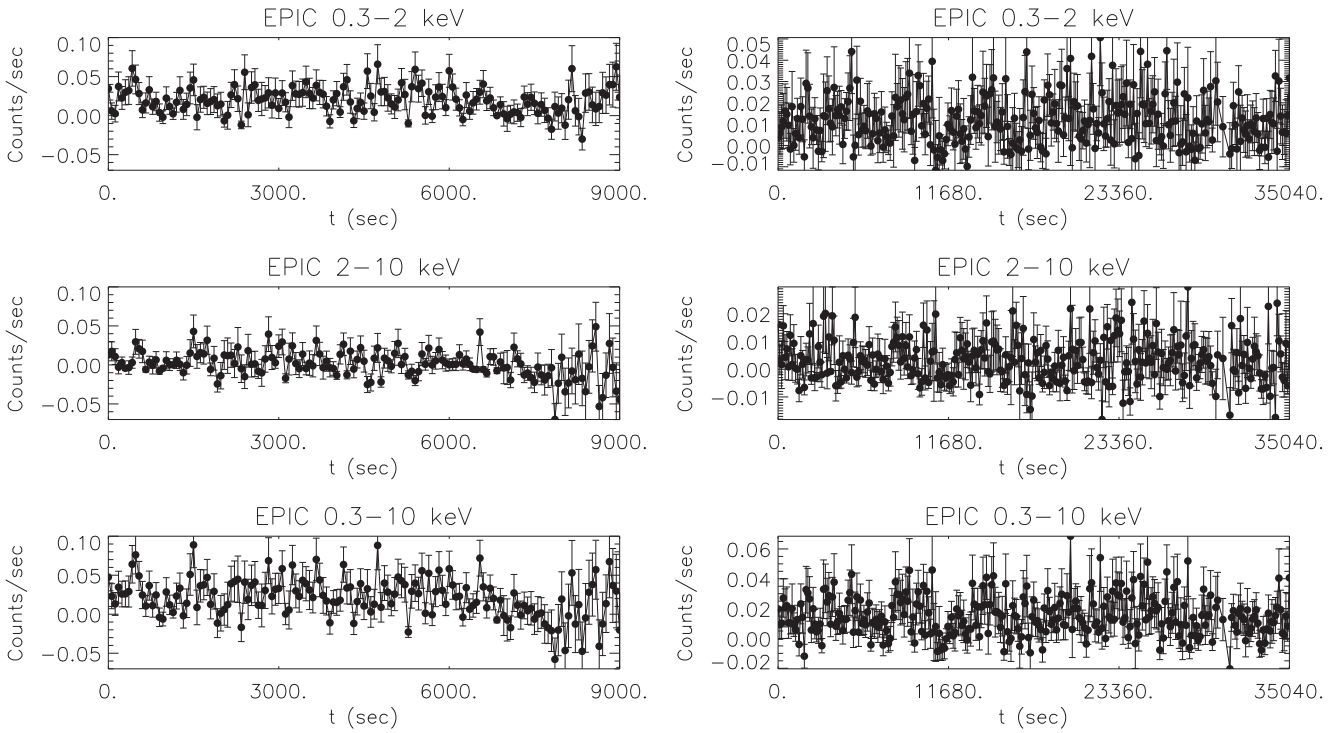

(a) (b)

Figure 2. Left-hand panel: the HP Cet Epic (background subtracted and synchronized) light curves in the 0.3–2 keV, 2–10 keV, and 0.3–10 keV bands, respectively. Each light curve has a bin size of 60 s and starts at MJD = 55941.9103 d. Right-hand panel: the light curve extracted for Swift J0820.6–2805 starting at MJD = 58226.3444 d. In this case, the light curve bin size was set to 120 s for graphical purposes. Each light curve is the average of the MOS 1, MOS 2, and pn (background subtracted and synchronized) light curves. See text for details.

By using the light curves with a bin size of 10 s and the Lomb–Scargle technique (Scargle 1982), we blindly performed a search for periodicities in the range between $2\Delta t$ (being Δt the time series bin size) and one-third of the observational window. Here, we conservatively require to have at least three full cycles for the maximum period tested. This requirement corresponds to a maximum period tested of $\simeq$50 and $\simeq$167 min for HP Cet and Swift J0820.6–2805, respectively.

The result of this analysis is shown in Fig. 3 for both HP Ceti and Swift J0820.6–2805. In each panel, we label the interesting periods identified by the method described above.

The optical light curve of HP Cet (also known as SDSS J0233) shows several modulations with short time-scales ranging from $\simeq$60 min up to 160 min (see e.g. Southworth et al. 2006 and references therein). Having determined spectroscopically a periodic feature at $\simeq$96 min, these authors tentatively interpret it as the CV

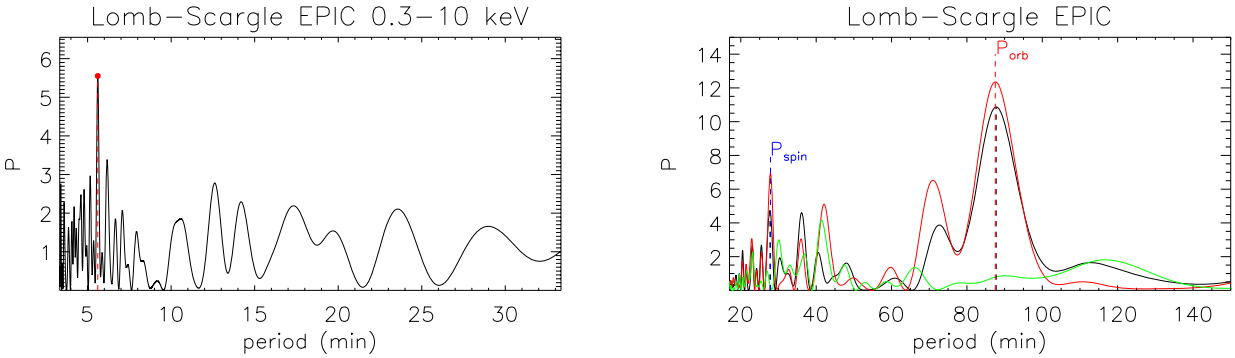

Figure 3. Left-hand panel: the Lomb–Scargle periodogram associated to the HP Cet light curve in the 0.3–10 energy band (10 s bin size). The red vertical line identifies the period found by the method described in the text and corresponds to ≃5.60 min. In the right-hand panel, we give the Lomb–Scargle periodogram for the soft (red), hard (green), and full (black) X-ray light curves. Here, we indicate the orbital period $P_{\rm orb}$ and tentatively identify the WD spin as the period at ≃27.87 min (see text for details).

orbital period and the signals at ≃60 and ≃160 min as the WD spin and the beat between orbital and spin period. Based on these periods, Southworth et al. (2006) classify HP Cet as an IP with a low accretion rate. This is in agreement with the X-ray variability observed by Szkody et al. (2002) with time-scale of ≃500 s as resulting from the analysis of *ROSAT* data. In this case, the author found that the source is active at the level of 0.0058 count s^{-1}. However, due to the quality of the *ROSAT* data, it was not possible to get any firm conclusion on the genuineness of the periodicity.

Since *XMM–Newton* data show a 0.3–10 keV rate of HP Cet (≃0.021 count s^{-1}) larger rate than in the *ROSAT* case, the variability or periodicity can be searched more easily. As clear from Fig. 3, panel (a), the Lomb–Scargle periodogram of the HP Cet light curve (in the energy band 0.3–10 keV) allows us to identify a clear peak at ≃5.60 min. The data folded at this period clearly show a repeated structure.

Due to the quality of the data and the conservative data-reduction procedure described in the previous section, the 0.3–10 keV time series of HP Cet do not allow to determine the orbital period of the source (≃96.08 min) neither the WD spin (tentatively identified with a periodic feature at ≃60 min; see Southworth et al. 2006) by using the high energy data alone (see in the following for details on the OM data analysis). The HP Cet light curve folded at ≃5.5 min (see Fig. 4, panel a) clearly shows a periodic sinusoidal structure. We tested the detected periodicity versus spurious features by computing the Lomb–Scargle periodograms of 5×10^4 fake light curves. For each light curve, we randomly shuffled the rate values while keeping the stamps of the time axis unchanged. Then, we define the false alarm probability (FAP) at a given tested period as the fraction (w.r.t. the total amount of simulations) of those periodograms having a power larger than that in the power spectrum observed at the same period. Therefore, the probability that a peak is genuine can be evaluated as $P = 1 - FAP$. When we apply this method to the HP Cet periodogram, we found that the ≃5.5 min has a probability of ≃99.5 per cent to be genuine.

As far as the source Swift J0820.6–2805 is concerned, the 0.3–10 keV light curve shows an average count rate of ≃0.015 count s^{-1}. The observational window of the target (≃35 ks) allows us to test longer periods by using the Lomb–Scargle technique. We searched for periodicities in the soft (0.3–2 keV), hard (2–19 keV), and full (0.3–10 keV) light curves independently and the resulting periodograms are given in panel (b) of Fig. 3 with red, green, and black lines, respectively. As in the case of other IPs, Swift J0820.6–2805 shows modulations in the soft band larger than in the hard band. X-ray signals are often characterized by modulations (Parker et al. 2005) on the WD spin $P_{\rm spin}$ and the orbital period $P_{\rm orb}$. In this case, we identify a strong peak, probably associated to the orbital period $P_{\rm orb} \simeq 87.53$ min, which almost disappears in the 2–10 keV band since the source is intrinsically fainter at these energies. The periodogram shows a second peak at ≃27.87 min that we tentatively associate with the spin period of the WD. Note that the power spin peak decreases in the hard band and appears again in the full band where the count rate is still dominated by the 0.3–2 keV photons. As clearly explained in Warner (1995), the presence of reprocessing sites and the existence of a modulation on the orbital period often induces the appearance of multiple orbital sidebands. In particular, we expect to find a sideband at $P_{\rm syn}^{-1} = P_{\rm spin}^{-1} - P_{\rm orb}^{-1}$ which, for the estimated values of spin and orbital periods, corresponds to $P_{\rm syn} \simeq$ 40.89 min which is close to the peak at ≃41.4–42.1 min[5] appearing in the periodogram. By considering the full width at half-maximum as the uncertainty associated to each of the estimated periods (with, in particular, 7 and 1 min for the orbital and spin periods, respectively), the observed feature appears to be consistent with the synodic period as expected.

We then folded the 0.3–10 keV light curve at the orbital period of ≃87.53 min and 60 bins per cycle and observed a clear sinusoidal pattern (see Fig. 4, panel b, where the zero phase is associated to the start for the *XMM–Newton* EPIC data at 55941.9098). Finally, having recognized the existence of such features, Swift J0820.6–2805 can be easily classified as a member of the IP class (see also Nucita et al. 2019, where the same method has been applied to the case of DW Cnc).

2.3 Timing analysis in the *UV* and *B* bands

HP Cet and Swift J0820.6–2805 have been observed by the OM on-board the *XMM–Newton* telescope in imaging and fast mode and by using the *UVM2* and *B* filters. We then binned the light curves in 10 s

[5]We note that a period of ≃41.4 min was found by Halpern & Thorstensen (2015) during one night observation and regarded as the possibe WD spin period.

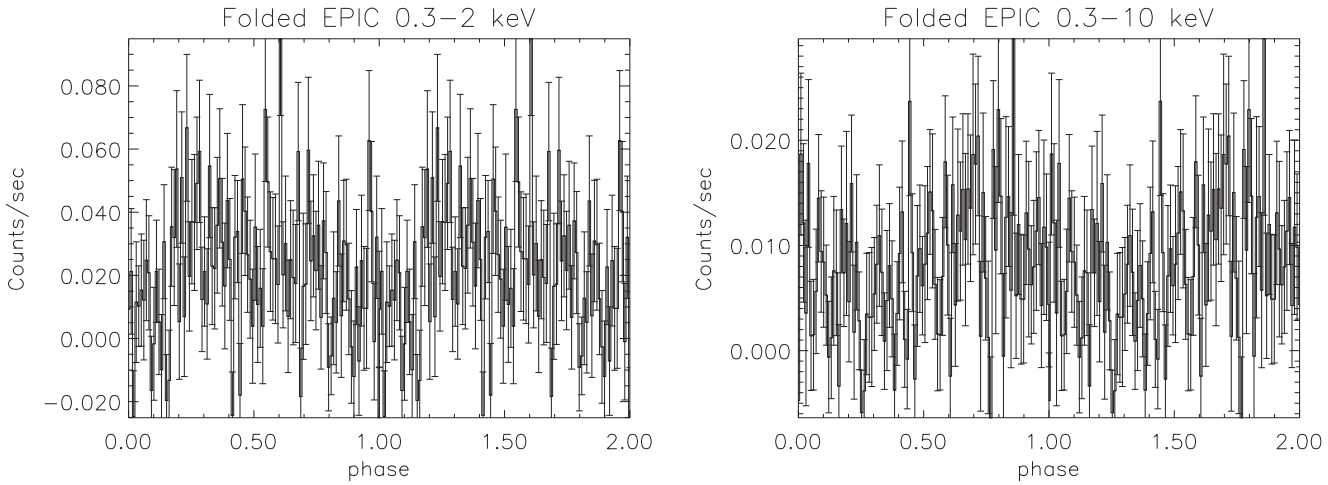

Figure 4. Left-hand panel: the folded light curve (with 60 s bins) of HP Cet over the period ≃5.5 min clearly shows a repeated structure. Right-hand panel: Here, we give the 0.3–10 keV light curve of Swift J0820.6–2805 when folded at the orbital period ≃87.53 min and with 60 s bins. In each panel, the zero phase bin is associated to the first entry in the corresponding light curve (see text for details).

wide bins and used the Lomb–Scargle method to search for periodic features.

In the case of HP Cet, the useful light curve (Fig. 5, left-hand panel) lasts for ≃5.6 h and has an average *UVM2* magnitude of ≃19.5. This allows us to search for any period up to ≃110 min when requiring to have at least three full cycles. The analysis resulted in the periodogram shown in Fig. 5 (right-hand panel) from which it is clear the presence of a rather broad peak at ≃88 min that is marginally consistent with the ≃96 min period found by Southworth et al. (2006) analyzing medium-resolution VLT/FORS2 spectroscopy of the source (see their Table 3). More interestingly, the periodogram shows a large peak at ≃58 min, i.e very close to the periodicity of approximately 60 min resolved by Southworth et al. (2006) and explained as the the possible WD spin period.

We performed a similar analysis for the source Swift J0820.6–2805 whose light curve (lasting for ≃9.5 h) in the *B* filter and with a bin size of 240 s is given in Fig. 6 (left-hand panel). The average magnitude of Swift J0820.6–2805 is 20.49. As one can note, the light curve seems to be characterized by a variability on time-scales of hundreds of minutes with, in particular, the appearance of two regions of large count rates at $t \simeq 22\,000$ and 30 000 s, respectively. This is also confirmed by the Lomb–Scargle periodogram which shows a rather wide feature at ≃130 min corresponding to the intrinsic variability of the source on this time-scale.

The light curves of the two sources were then folded at the relevant period found with the Lomb-Scargle analysis. In particular, in Fig. 7 (left-hand panel), we present two cycles of the HP Cet light curve (OM *UVM2* filter) folded over the 88 min and setting the zero phase bin to the starting time of the EPIC 0.3–10 keV light curve (with 10 s bins), i.e. MJD = 55941.9098. For Swift J0820.6–2805, the existence of a long term variability is also confirmed when folding the light curve at 130 min (see right-hand panel in Fig. 7 where we set the zero phase bin to the starting time – MJD = 58226.3432 – of the EPIC 0.3–10 keV light curve with 10 s bins).

.

2.4 Spectral analysis

HP Cet and Swift J0820.6–2805 are very faint sources, as it is clear from the average count rate in the 0.3–10 keV band of ≃0.02 count s^{-1} and 0.015 count s^{-1}, respectively. For HP Cet, we extracted the spectrum for the source and background regions along with the response matrix files for MOS 1, MOS 2, and pn cameras. We then binned the spectra with the GRPPHA tool by requiring to have at least 25 counts per energy bin. The spectra were imported within the XSPEC package (version 12.9.0) for the spectral analysis and fitting procedure (see Fig. 8).

Due to the low count rate, the HP Cet spectrum is of poor quality. We first tried to fit it with a MEKAL model describing the emission from a hot diffuse gas (Mewe, Gronenschild & van den Oord 1985) with the inclusion of emission lines from several elements. The estimated distance to HP Cet, as reported in the second data release of the Gaia telescope measurements (see Brown et al. 2018), is ≃600 pc, so that we fixed the redshift parameter to zero and the material abundances to the solar values. We also accounted for any possible absorption by considering a multiplicative component PHABS, which depends on the energy as $\exp(-NH\sigma(E))$, where *NH* is neutral hydrogen column density and $\sigma(E)$ is the photoelectric cross-section. The initial value of *N* was set to the value observed towards the target and provided by Kalberla et al. (2005), i.e. $NH \simeq 0.0281 \times 10^{22}$ cm^{-2}. The best fit ($\chi^2 = 1.1$ for 172 d.o.f.) converged towards a MEKAL temperature of $kT_{\rm mk} = 3.9^{+1.5}_{-0.9}$ and an upper limit on the neutral hydrogen column density of $NH < 0.014 \times 10^{22}$ cm^{-2}. Finally, the unabsorbed 0.3–10 keV band flux is $(1.3^{+0.2}_{-0.2}) \times 10^{-13}$ erg s^{-1} cm^{-2}. By using the above distance, the intrinsic luminosity is estimated to be $\simeq 5 \times 10^{30}$ erg s^{-1} in the above-mentioned band.

Although Swift J0820.6–2805 has approximately the same count rate as HP Cet, the longer observation, and the absence of strong solar flares, allowed to collect a larger number of photons which, in turn, enabled us to produce a 0.3–10 keV spectrum of acceptable quality. We extracted the spectrum of the source, corrected it for the background and exposure and binned the result in order to have at least 25 counts per energy bin. The resulting spectra for MOS 1 (red), MOS 2 (green), and pn (black) cameras are shown in Fig. 9.

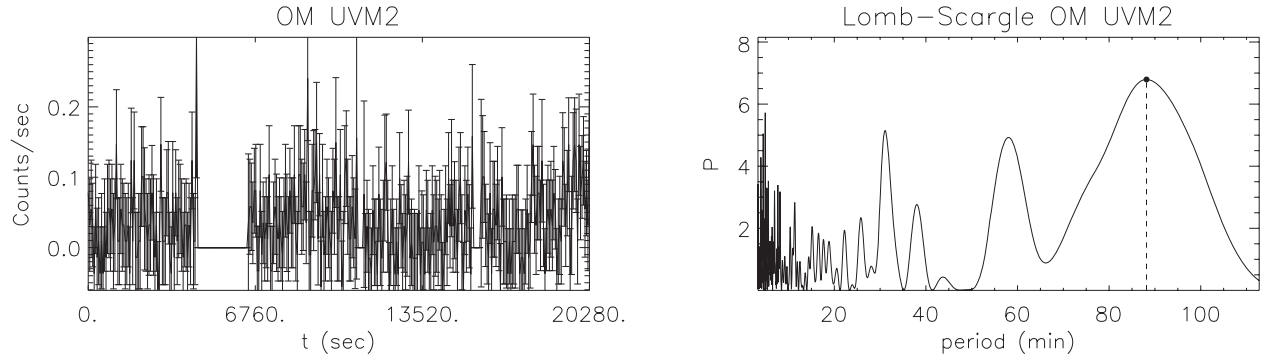

(a) (b)

Figure 5. Left-hand panel: the OM light curve (*UVM2* filter) of HP Cet with a 60 s bin size. In the right-hand panel, we give the Lomb–Scargle periodogram with the identification of a $\simeq$88 min period with a confidence level of 1σ. The large peak at $\simeq$58 min is very close to the periodicity of approximately 60 min resolved by Southworth et al. (2006) and possibly associated to the WD spin period.

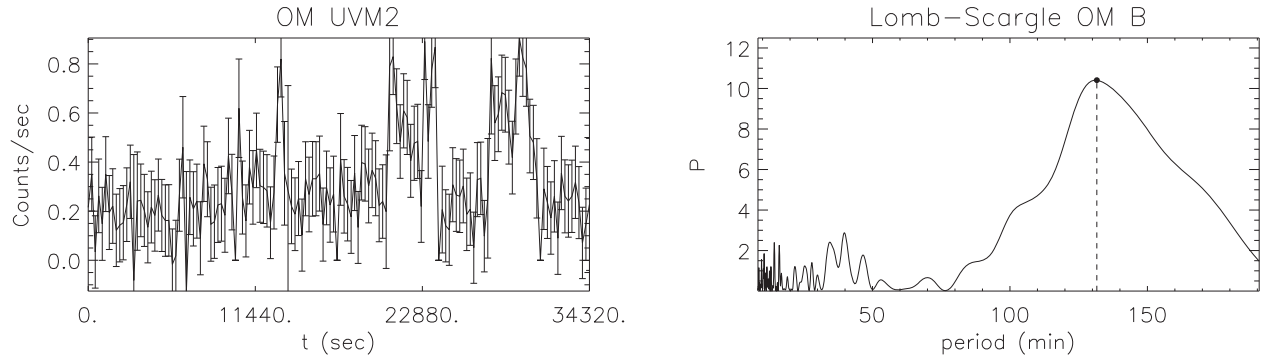

(a) (b)

Figure 6. In the left-hand panel, we give the OM light curve (*B* filter) of Swift J0820.6–2805 with a 240 s bin size. The right-hand panel shows the Lomb–Scargle periodogram with the identification of a $\simeq$131 min period (see text for details).

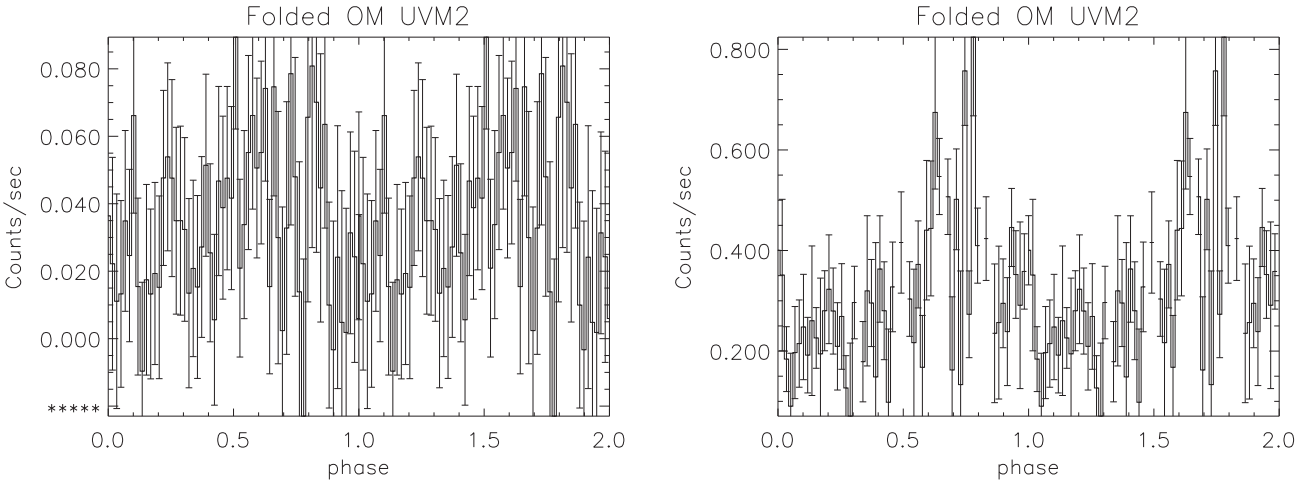

(a) (b)

Figure 7. In the left-hand panel, we give the OM light curve folded over the 88 min of HP Cet. In the right-hand panel, the folding of the Swift J0820.6–2805 time series is performed over the variability of $\simeq$130 min detected in the *B* band.

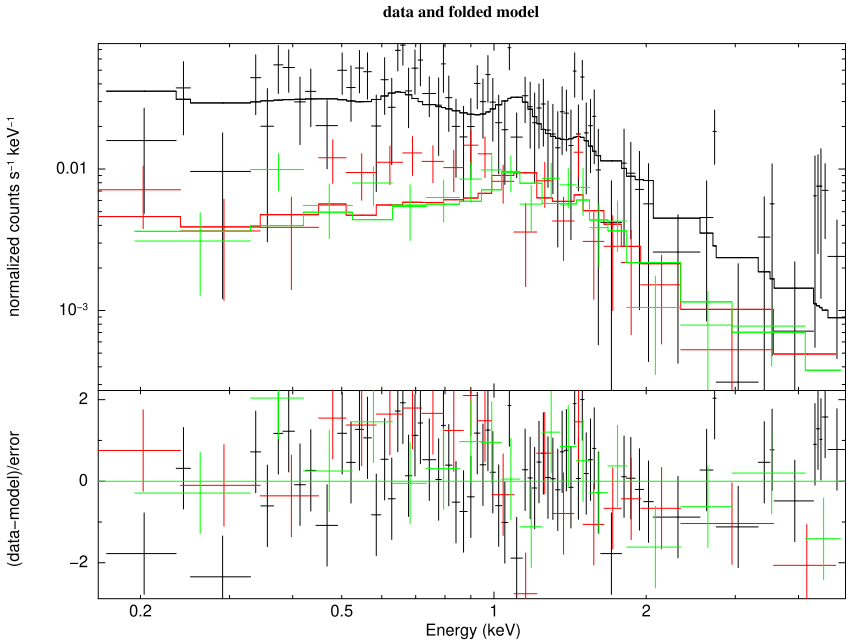

Figure 8. The 0.3–4 keV spectra for the MOS 1 (red), MOS 2 (green), and pn (black) data of HP Cet together with the best-fitting model (see text for details) are presented.

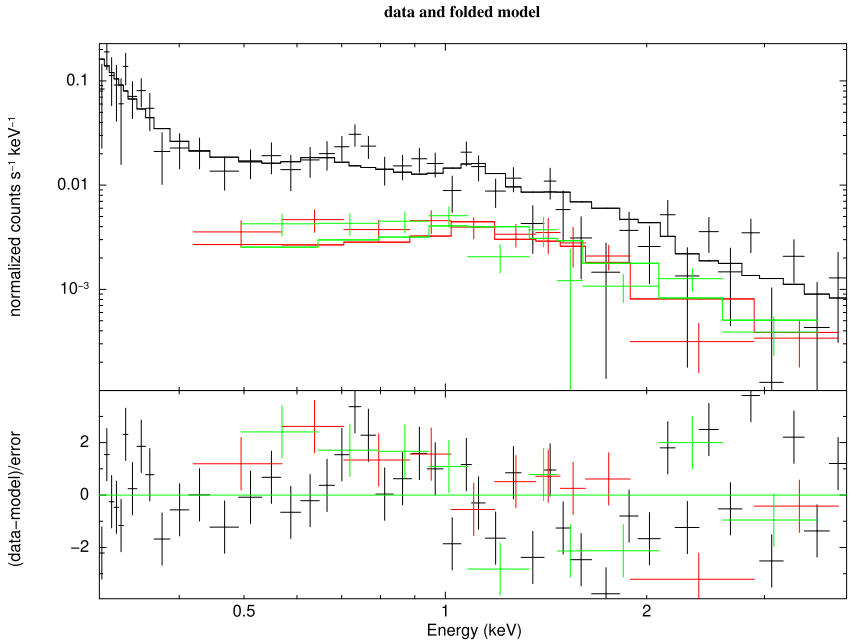

Figure 9. The 0.3–4 keV spectra for the MOS 1 (red), MOS 2 (green), and pn (black) data of Swift J0820.6–2805 along with the best-fitting model (see text for details) are shown.

By using XSPEC, we started by fitting the data with a single MEKAL model. As before, since the source is at a distance of $\simeq$200 pc (Parisi et al. 2014), we fixed the redshift parameter to zero and the abundances to the solar values. Note that the data show a clear excess of photons at low energies suggesting that the absorption due to the hydrogen column density *NH* is likely to be small and that a soft spectral component is required in order to obtain a good fit. In fact, a single MEKAL component (not absorbed by any intervening matter) was unable to adequately fit the data (χ^2 larger than 2.5) and, consequently, we added a second thermal component (a BBODYRAD model) to the previous one.

The best-fitting procedure (with reduced $\chi^2 = 1.5$ for 63 d.o.f) resulted in the MEKAL and blackbody temperatures of $kT_{\rm mk} = 3.9^{+1.5}_{-0.9}$ keV and in $kT_{\rm bb} = (2.12^{+0.6}_{-0.5}) \times 10^{-2}$ keV, respectively. Note that the errors are quoted at the 90 per cent confidence level. The estimated MEKAL normalization results to be $N_{\rm mk} = (3.85^{+0.36}_{-0.34}) \times 10^{-5}$ in units of $10^{-14} \int n_{\rm e} n_{\rm H} {\rm d}V / 4\pi [D_{\rm A}(1+z)]^2$, where $D_{\rm A}$ is the angular diameter of the source, $n_{\rm e}$ and $n_{\rm H}$ the electron and hydrogen density,

and the integral is on the emission volume. For the blackbody component, the associated normalization $N_{\rm bb} = (1.3^{+89.0}_{-1.3}) \times 10^7$ is given in units of $R^2_{\rm km}/D^2_{10\ \rm kpc}$, where $R_{\rm km}$ is the radius (in kilometers) of the X-ray emitting region and $D_{10\,\rm kpc}$ is its distance in units of 10 kpc. Hence, for the assumed distance to the target, the equivalent radius of the source emitting region is in the range 12–600 km, i.e. much smaller than the radius of the WD itself. We emphasize that Worpel & Schwope (2015) found a quite similar result analyzing the polar CV labelled as CSS081231:071126+440405. We then determined the upper limit of the hydrogen column density that absorbs the X-ray flux by introducing a PHABS component in XSPEC. In particular, we increased the value of *NH* (e.g. by using the *steppar* command in XSPEC) until no statistically acceptable fit could be obtained, i.e. when the χ^2 value changed to 2.7 with respect to the value obtained by the best fit. This procedure resulted in a 90 per cent upper limit of $0.0075 \times 10^{22}\,{\rm cm}^{-2}$, i.e. well below the average galactic column density of $0.293 \times 10^{22}\,{\rm cm}^{-2}$ towards the target (Kalberla et al. 2005). Below the estimated upper limit, the fit is essentially insensible to the *NH* value since the absorption is simply not required.

Finally, we evaluated the unabsorbed 0.3–10 keV band flux of the source to be $(7.8^{+0.5}_{-2.6}) \times 10^{-14}\,{\rm erg\,s^{-1}\,cm^{-2}}$ corresponding to an intrinsic luminosity of $\simeq 3.8 \times 10^{29}\,{\rm erg\,s^{-1}}$. This appears to be one of the lowest luminosity IPs in X-rays.

3 DISCUSSION AND RESULTS

IPs are CVs, i.e. binary systems in which a strongly magnetized WD (with magnetic field of up to $\simeq$10 MG) accretes matter from a donor star. The radially infalling material produces a shock wave above the magnetic pole on the surface of the primary star. As a consequence, IPs emit X-rays originating from hot plasma with temperature up to 20–50 keV. Depending on the physical parameters of the accretion gas column, the X-ray spectrum can show either cooling flows or photoionization components (see e.g. Mukai, Still & Ringwald 2003) which, in addition, might be absorbed by the intervening matter, being the suppression strongly dependent on the actual geometry of the system. In this respect, satellites with large sensitivity (as *XMM–Newton*) allow to discover and study a population of soft IPs characterized, for example, by blackbody components with low plasma temperature ($kT \simeq 50$ eV).

Although IPs are expected to be common in the Milky Way, they are difficult to detect because either they are intrinsically faint or they suffer of absorption. Nowadays, it appears quite clear that faint IPs do exist. In fact, Pretorius & Mukai (2014) showed that, while most of the detected hard IP sources are characterized by a typical luminosity of $\simeq 10^{33}\,{\rm erg\,s^{-1}}$, there is evidence of the existence of a rather rare faint population. Among the elusive sources (with luminosity less than $\simeq 10^{32}\,{\rm erg\,s^{-1}}$), only a few were observed in the soft (AE Aqr, DQ Her, and V902 Mon) and hard (DO Dra, V1025 Cen, and EX Hya) band. Apparently, two unconfirmed IPs (V597 Pup and V475 Sgr, see Worpel et al. 2020) are at the lower end of this distribution since the source estimated luminosities are of the order of $10^{31}\,{\rm erg\,s^{-1}}$).

As observed by Gänsicke et al. (2005; but see also Aungwerojwit et al. 2012), IPs above the period gap (2–3 h) are characterized by a ratio of $P_{\rm spin}/P_{\rm orb}$ widely distributed in the range 0.01–0.1, while all the systems below the gap have $P_{\rm spin}/P_{\rm orb} > 0.1$. Furthermore, since most of the known IP have orbital periods above the gap, it has been suggested that IPs evolve to polars becoming synchronized (Chanmugam & Ray 1980). Of course, if the subclass of low luminosity IP contains short period systems then short period IPs should be intrinsically common as polars. In this case, there is the possibility that long period IP can evolve through the period gap simply becoming short period IPs.

In this work, we reported on the timing analysis of X-ray data from two CVs of interest, HP Cet and Swift J0820.6–2805, which are classified as IP candidate and, as such, listed in IPhome catalogue. The *XMM–Newton* observations for HP Cet (ID 673140201) and Swift J0820.6–2805 (ID 0801780401) were not previously analyzed and, in particular, a confirmation of the IP nature for Swift J0820.6–2805 was missing. Our analysis of the 0.3–10 keV band and UV data of HP Cet confirms the existence of a periodicity of $\simeq$88 min that we address as the orbital period. Note that this is slightly different from the value of $\simeq$96 min reported by Southworth et al. (2006). We also detected a periodic signal at $\simeq$5.6 min that seems to be a genuine feature. Note that a close variability of about 8 min was found by Szkody et al. (2002) analysing past *ROSAT* satellite data.

In the case of the IP candidate Swift J0820.6–2805, we showed that the high energy light curve is characterized by a periodic signal on the scale of the orbital period ($\simeq$87.77 min). We clearly identified also the spin period of the WD (at $\simeq$27.87 min) with the typical sidebands expected for magnetic systems, thus allowing us to confirm the IP nature of the source. Moreover, the analysis of the *B* band light curve showed also the existence of a $\simeq$130 min variability that needs to be confirmed by further dedicated follow-up observation.

Both HP Cet and Swift J0820.6–280 appear to be underluminous sources in X-ray since, for the estimated distances of 600 and 200 pc, they have luminosities of $\simeq 5 \times 10^{30}$ and $\simeq 3.8 \times 10^{29}\,{\rm erg\,s^{-1}}$, respectively. The low luminosity appear to be due to the intrinsic accretion mechanism since the targets show a negligible absorption. The two IPs in question are particularly interesting not only because they are characterized by a very low luminosity but also because their orbital period appears to be well below the so-called period gap. These IPs appear to be members of a currently poorly populated class (which, in reality, could be the most numerous) formed by short period and low luminosity IPs which probably evolved from the long period stage to the short period one. Confirming this scenario requires the discovery and study of other objects of this class and constitutes a challenging research subject.

ACKNOWLEDGEMENTS

This paper is based on observations from *XMM–Newton*, an ESA science mission with instruments and contributions directly funded by ESA Member States and NASA. We thank for partial support the INFN projects TAsP and EUCLID. We also acknowledge the anonymous referee for several suggestions which allowed to improve this paper and for spotting a crucial error in the performed analysis.

4 DATA AVAILABILITY

The data underlying this article were accessed from the *XMM–Newton* Science Archive (http://nxsa.esac.esa.int/nxsa-web/#home, ID 673140201 and 0801780401). The derived data generated in this research will be shared on reasonable request to the corresponding author.

REFERENCES

Aungwerojwit A. et al., 2012, ApJ, 758, 79
Balman S., 2011, ApJ, 741, 84
Baumgartner W. H. et al., 2013, ApJS, 207, 19
Brown A. G. A. et al., 2018, A&A, 616, A1
Chanmugam G., Ray A., 1984, ApJ, 285, 252

Cusumano G. et al., 2010, A&A, 524, A64
Gänsicke B. T. et al., 2005, MNRAS, 361, 141
Halpern J. P., Thorstensen J. R., 2015, AJ, 150, 170
Hoard D. W. et al., 2010, AJ, 140, 1313
Kalberla P. M. W. et al., 2005, A&A, 440, 775
Kuulkers E., Norton A., Schwope A., Warner B., 2006, Compact Stellar X-ray Sources, Cambridge Univ. Press, Cambridge , 421
Mewe R., Gronenschild E. H. B. M., van den Oord G. H. J., 1985, A&AS, 62, 197
Mukai K., 2017, PASP, 2017, 129
Mukai K., Still M., Ringwald F., 2003, ApJ, 594, 428
Nucita A. A. et al., 2009a, New Astron., 14, 302
Nucita A. A. et al., 2009b, A&A, 504, 973
Nucita A. A. et al., 2011, A&A, 536, A75
Nucita A. A. et al., 2014, A&A, 566, 121
Nucita A. A., Conversi L., Licchelli D., 2019, MNRAS, 484, 3119
Parisi P. et al., 2014, A&A, 561, A67
Parker T. L., Norton A. J., Mukai K., 2005, A&A, 439, 213
Pretorius M. L., Mukai K., 2014, MNRAS, 442, 2580
Ramsay G. et al., 2004, MNRAS, 350, 1373
Revnivtsev M. et al., 2009, Nature, 458, 1142
Scargle J. D., 1982, ApJ, 263, 835
Southworth J. et al., 2006, MNRAS, 373, s687
Szkody P. et al., 2004, AJ, 123, 430
Szkody P. et al., 2004, AJ, 128, 2443S
van Teeseling A., Beuermann K., Verbunt F., 1996, A&A, 315, 467
Warner B., 1995, Cataclysmic Variable Stars, Cambridge Univ. Press, Cambrige
Warwick R. S., Byckling K., Pérez-Ramírez D., 2014, MNRAS, 438, 2967
Worpel H., Schwope A. D., 2015, A&A, 583, A130
Worpel H., Schwope A. D., Traulsen I., Mukai K., Ok S., 2020, A&A, 639, A17
Worrall D. M., Marshall F. E., Boldt E. A., Swank J. H., 1982, ApJ, 255, 111
XMM-Newton Science Analysis System, 2019, ESA: XMM-Newton SOC, Available at: https://xmm-tools.cosmos.esa.int/external/xmm_user_support/documentation/sas_usg/USG/

This paper has been typeset from a TEX/LATEX file prepared by the author.